OL Organic Letters

pubs.acs.org/OrgLett Letter

Genome Mining of a Deep-Sea-Derived *Penicillium allii-sativi* Revealed Polyketide-Terpenoid Hybrids with Antiosteoporosis Activity

Chun-Lan Xie,[#] Tai-Zong Wu,[#] Yuan Wang, Robert J. Capon, Ren Xu, and Xian-Wen Yang*

Cite This: *Org. Lett.* 2024, 26, 3889−3895 Read Online

ACCESS | Metrics & More | Article Recommendations | Supporting Information

ABSTRACT: Two novel meroterpenoids, alliisativins A and B (**1**, **2**) were discovered through a genome-based exploration of the biosynthetic gene clusters of the deep-sea-derived fungus *Penicillium allii-sativi* MCCC entry 3A00580. Extensive spectroscopic analysis, quantum calculations, chemical derivatization, and biogenetic considerations were utilized to establish their structures. Alliisativins A and B (**1**, **2**) possess a unique carbon skeleton featuring a drimane sesquiterpene with a highly oxidized polyketide. Noteworthily, alliisativin A (**1**) showed dual activity in promoting osteogenesis and inhibiting osteoclast, indicating an antiosteoporosis potential.

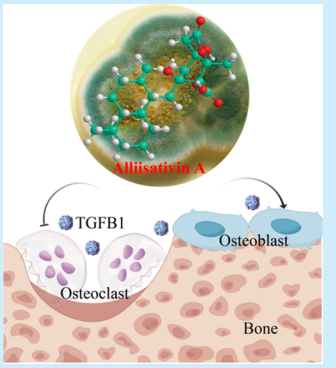

Filamentous fungi from the ocean remain an abundant source of secondary compounds with various biological activities.[1] With genome sequencing techniques, numerous natural-product-related biosynthetic gene clusters have been identified. Complex natural products can be generated via biosynthetic pathways that include several key enzymes. Fungi produce complex hybrid natural products by combining various core enzymes in the same biosynthetic pathway, like PKS/PKS, PKS/NRPS, and PKS/TC, which cannot be achieved with only one core enzyme.[2]

Cyclohexane-connected drimane sesquiterpenes are a group of compounds consisting of a drimane-type sesquiterpene structure attached to a cyclohexanone or cyclopentane group. Being relatively uncommon in nature,[3] cyclohexane sesquiterpenes have sparked significant interest among synthetic chemists because of their appealing biological properties.[4] For instance, epoxyphomalin A displayed a superior cytotoxicity at nanomolar concentrations toward 12 of a panel of 36 human tumor cell lines,[5] while macrophorins were documented with antifungal activity.[6] Yi Tang and colleagues discovered the biosynthetic gene cluster responsible for producing epoxycyclohexenone macrophorins by utilizing genome mining techniques, confirming the *MacJ* gene cluster as the initial integral membrane terpene cyclase capable of cyclizing terpenes by directly protonating olefinic bonds.[7] Interestingly, a similar gene cluster was discovered in *Penicillium allii-sativi* MCCC 3A00580, a deep-sea-derived fungus. Accordingly, genome exploration was conducted, followed by the isolation and purification of three polyketide-terpenoid hybrids (**1**−**3**, Figure 1) through HRMS and UV guidance. Herein, we report the isolation, structure, and biological effects of these isolates.

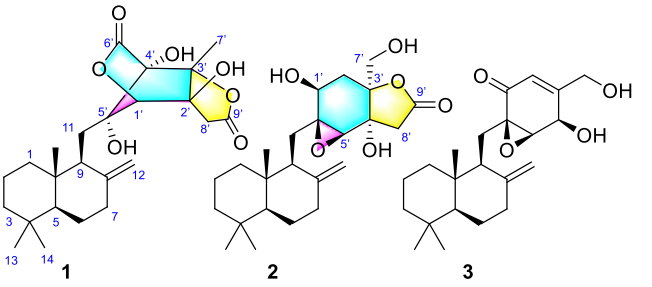

Figure 1. Compounds **1**−**3** isolated from *Penicillium allii-sativi* MCCC 3A00580.

The whole genome sequence of MCCC 3A00580 was submitted to antiSMASH for the secondary metabolites biosynthetic gene clusters (BGCs) analysis. A total of 40 BGCs were discovered in this strain, comprising 12 type I polyketide synthases (T1PKSs), seven nonribosomal peptide synthetases (NRPSs), six terpene cyclases (TCs), 11 NRPS-like, one indole-NRPS, two T1PKS-NRPS, and one β-lactone

Received: March 24, 2024
Revised: April 23, 2024
Accepted: April 23, 2024
Published: April 26, 2024

https://doi.org/10.1021/acs.orglett.4c01065
Org. Lett. 2024, 26, 3889−3895

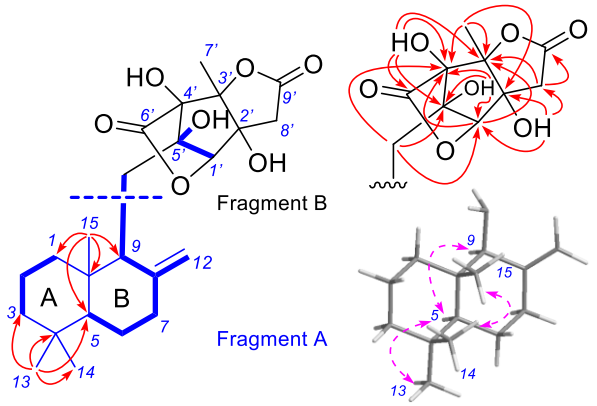

Figure 2. Selected COSY (blue line), HMBC (red arrow), and NOESY (pink arrow) correlations of **1**.

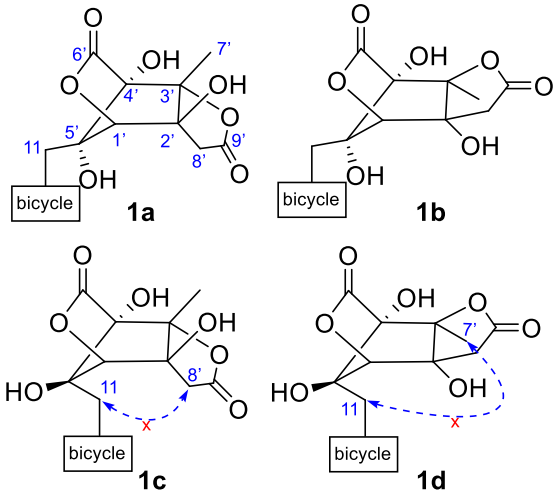

Figure 3. Possible diastereoisomers of **1** with NOESY correlations drawn in the blue dotted line.

gene clusters. Among these, a single gene cluster (termed herein *Mer*) of 3A00580 was identified with genes predicted as a T1PKS gene cluster, involved in the biosynthesis and secretion of the yanuthones and macrophorins (Figure S1). BLAST analyses revealed a significant similarity (70%) between the *Mer* gene clusters and the *yan* gene clusters from *Aspergillus niger* ATCC 1015. The linear compound

Table 1. ^{1}H and ^{13}C NMR Spectroscopic Data for Compounds 1 and 2 (δ in ppm, J in Hz within the Parentheses)

	1[a]		**2**[a]		**2**[b]	
Pos.	δ_H	δ_C	δ_H	δ_C	δ_H	δ_C
1	1.63 td (13.2, 3.0)	38.1 CH_2	1.66[c]	38.4 CH_2	1.63 d (12.0)	38.8 CH_2
	1.07 td (13.2, 3.0)		0.95 td (13.3, 4.1)		1.03 td (12.0, 4.0)	
2	1.50 m; 1.42 td (13.9, 3.7)	18.8 CH_2	1.50 dd (14.0, 10.5); 1.44 m	18.9 CH_2	1.63;[c] 1.54[c]	19.2 CH_2
3	1.35 m; 1.13 m	41.8 CH_2	1.35 d (13.0); 1.16 dd (13.0, 3.4)	41.7 CH_2	1.40 m; 1.21 m	41.9 CH_2
4		41.4 C		41.0 C		42.0 C
5	1.15 s	55.0 CH	1.12 td (13.0, 2.0)	54.8 CH	1.18 d (15.0)	55.7 CH
6	1.72 m	24.0 CH_2	1.67[c]	23.7 CH_2	1.83 d (12.5)	24.8 CH_2
	1.24 m		1.23 m		1.35 dd (12.5, 4.0)	
7	2.34 td (12.8, 2.3)	37.9 CH_2	2.33 d (13.0)	37.4 CH_2	2.48 d (12.7)	38.4 CH_2
	2.03 td (12.8, 4.7)		1.96 m		2.10 td (12.7, 4.0)	
8		149.0 C		149.2 C		152.8 C
9	2.13 d (9.0)	49.7 CH	1.52 d (10.5)	50.7 CH	1.91 d (9.0)	52.5 CH
10		40.0 C		38.9 C		40.2 C
11	1.72 d (15.3)	24.1 CH_2	2.04 dd (15.2, 9.6)	23.5 CH_2	2.27 dd (15.4, 9.0)	25.3 CH_2
	1.38 dd (15.3, 9.0)		1.80 d (15.2)		1.58, 9.0	
12	4.78 s; 4.52 s	106.2 CH_2	4.78 s; 4.52 s	106.2 CH_2	4.76 s; 4.94 s	105.6 CH_2
13	0.85 s	33.4 CH_3	0.85 s	33.3 CH_3	0.88 s	33.4 CH_3
14	0.76 s	21.4 CH_3	0.76 s	21.6 CH_3	0.79 s	21.5 CH_3
15	0.57 s	14.6 CH_3	0.61 s	19.7 CH_3	0.66 s	14.7 CH_3
1′	4.15 s	81.4 CH	3.96 br s	66.0 CH	4.22 br s	66.4 CH
2′		79.5 C	1.98 dd (14.0, 3.5)	32.0 CH_2	1.97 m	35.7 CH_2
			1.48 dd (14.0, 3.5)		1.93 m	
3′		88.9 C		87.1 C		84.4 C
4′		86.6 C		73.6 C		74.9 C
5′		83.4 C	2.90 s	61.6 CH	3.17 br s	64.1 CH_2
6′		173.8 C		62.7 C		63.9 C
7′	1.18 s	16.7 CH_3	3.70 d (12.2); 3.65 d (12.2)	63.3 CH_2	3.91 s	67.0 CH_2
8′	3.00 d (18.2); 2.58 d (18.2)	41.3 CH_2	2.89 d (17.7); 2.53 d (17.7)	41.0 CH_2	3.07 d (18.0); 2.72 d (18.0)	40.1 CH_2
9′		174.2 C		174.2 C		173.8 C
1′-OH			5.47 br s			
2′-OH	5.85 d (2.7)					
4′-OH	6.50 br s		5.81 s			
5′-OH	5.74 s					

[a]Measured in DMSO-d_6. [b]Measured in $CDCl_3$. [c]overlapped

https://doi.org/10.1021/acs.orglett.4c01065
Org. Lett. 2024, 26, 3889−3895

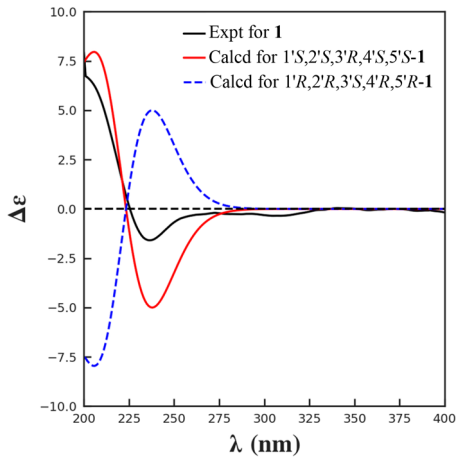

Figure 4. Calculated and experimental ECD spectra of **1**.

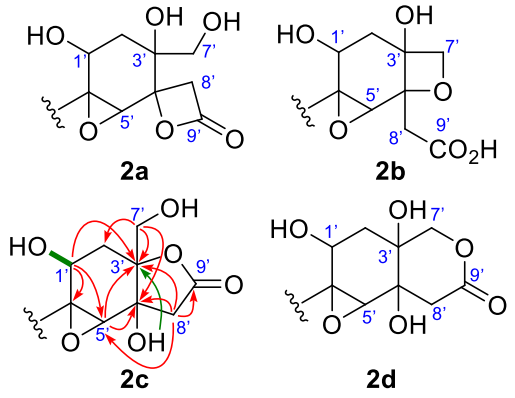

Figure 5. Possible substructures of **2** with 2D NMR correlations inset (red arrow, HMBC correlations observed in $CDCl_3$; green arrow, HMBC correlations observed in DMSO-d_6; green line, COSY correlations observed in DMSO-d_6).

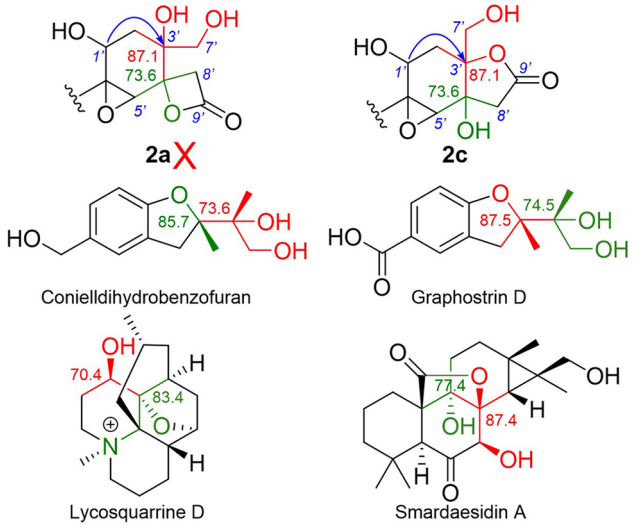

Figure 6. NMR chemical shifts comparison of compound **2** (in DMSO-d_6) with referenced compounds (blue arrow, HMBC correlations observed in DMSO-d_6).

yanuthone, featuring a cyclohexenone ring, is derived from 6-methylsalicylic acid (6-MSA), synthesized by a ten-gene cluster including *yan* A and *yan* I. In contrast, the *mac* cluster contains

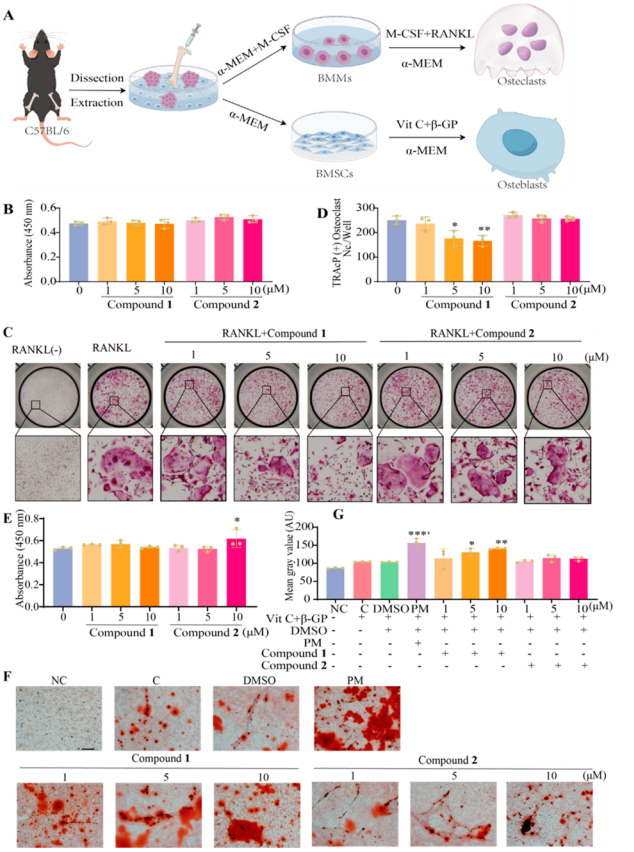

Figure 7. Compounds **1** and **2** suppress RANKL-induced osteoclastogenesis in BMMs and increase osteogenic mineralization activity among BMSCs in a dose-dependent manner. (A) Schematic diagram of the osteogenesis and osteoclast differentiation process. (B) The cytotoxicity of compounds **1** and **2** on BMMs was measured by a CCK-8 assay (n = 3). (C) Representative images of osteoclasts following treatment with RANKL and either compound **1** or **2** at concentrations of 0, 1, 5, and 10 μM. Scar bar = 1000 μm (n = 3). (D) Quantitative assessment of tartrate-resistant acid phosphatase (TRAcP)-positive multinucleated cells (>3 nuclei) per well. (E) The cytotoxicity of compounds **1** and **2** on BMSCs was measured by an CCK-8 assay (n = 3). (F) Osteogenic mineralization activity among BMSCs was stained with Alizarin red S after treating with the indicated concentrations of compounds **1** and **2** (n = 3). (G) Quantification of Alizarin red S staining area based on average optical density. The culture medium, osteogenesis differentiation medium (50 μg/mL ascorbic acid and 5 mM β-glycerophosphate (β-GP), DMSO (0.1%), and purmorphamine (1 μM) were regarded as the negative control (NC), control (C), solvent (DMSO), and positive control groups (PM), respectively. Scar bar = 250 μm. All bar graphs are presented as the mean ± SD *P < 0.05; **P < 0.01; ***P < 0.001; ****P < 0.000 1 vs the DMSO group.

a single gene insertion compared to the *yan* cluster. The conversion of the linear chain in yanuthones to the drimane unit in macrophorins is facilitated by the *MacJ*. Therefore, it is plausible that the *Mer* gene clusters are involved in the biosynthesis of polyketide-sesquiterpene hybrids. The functions of open reading frames (ORFs) in *Mer* from 3A00580 were deduced (Table S1).

The chemical investigation on the fungus MCCC 3A00580 was subsequently conducted. As a result, two novel meroterpenes (**1**, **2**) and one known derivative (**3**) were obtained from its CH_2Cl_2-soluable extract using multiple column chromatography (CC) over ODS, silica gel, and

https://doi.org/10.1021/acs.orglett.4c01065
Org. Lett. 2024, 26, 3889−3895

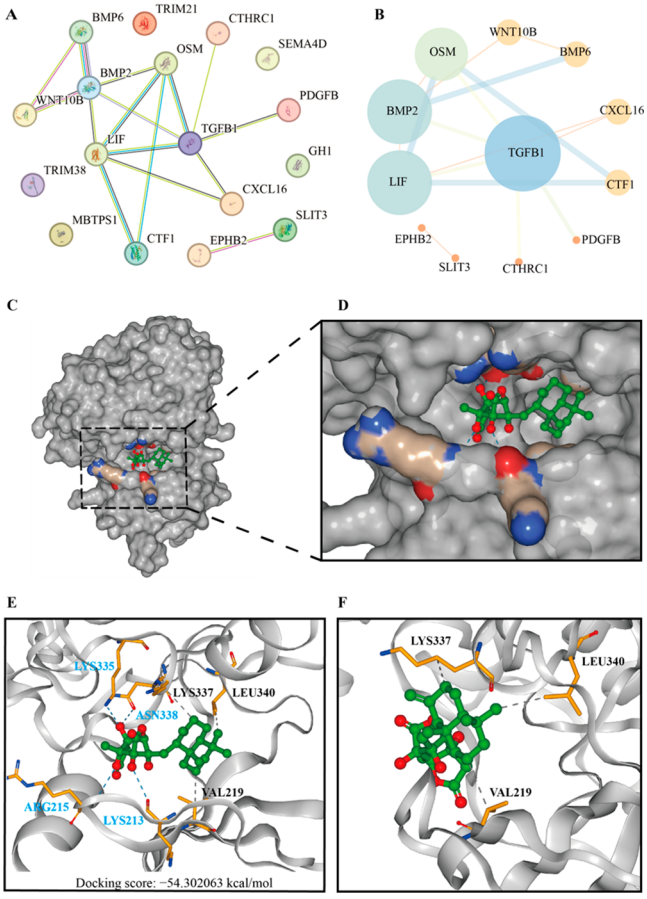

Figure 8. Compound **1** can bind to TGFB1 (PDB ID: 4X2F) protein. (A) The protein interaction network of factors involved in the coupling of osteoblasts and osteoclasts was constructed using data from refs 13b and 17a. The PPI network was constructed with the String database version 12.0. (B) The PPI network was visualized and analyzed by using Cytoscape 3.7.0 and 3.9.1. A node in a network graph symbolizes a specific target, with its size and color serving as visual indicators of the degree value. A color gradient from blue to yellow to orange signifies a progression from low to high degree values, while larger nodes correspond to higher degree values. (C) 3D structure of compound **1** with TGFB1 complex. (D) A detailed view of 3D structure of compound **1** with TGFB1 complex. (E) Hydrogen bonds and hydrophobic interactions of compound **1** with neighboring amino acid residues in TGFB1. (F) The hydrophobic interactions of compound **1** with protein TGFB1.

Sephadex LH-20. By comparing the NMR and HRMS spectra with previously published data, together with a X-ray diffraction analysis (Figure S24), compound **3** was unambiguously determined as macrophorin A.[8]

The HRMS analysis of **1** returned a molecular formula as $C_{24}H_{34}O_7$, indicating eight degrees of unsaturation. Its ^1H and ^{13}C NMR spectroscopic data (Table 1) revealed four methyl singlets, seven sp^3 methylene, one sp^2 methylene, three methine, and nine non-hydrogenated carbons. Analysis of the 2D NMR spectra of **1** allowed the connection of the fragment A, which was similar to the drimane moiety of macrophorin A (**3**), evident from the HMBC correlations of H_3-13 (δ_H 0.85 s)/H_3-14 (δ_H 0.76 s) to C-3/4/5, H_3-15 (δ_H 0.57 s) to C-1/5/9/10, and COSY correlations of H-5 (δ_H 1.15 m)/H_2-6 (δ_H 1.72 m; 1.24 m)/H_2-7 (δ_H 2.34 td, J = 12.8, 2.3 Hz; 2.03 td, J = 12.8, 4.7 Hz)/H_2-12 (δ_H 4.78 s; 4.52 s)/H-9 (δ_H 2.13 d, J = 9.0 Hz)/H_2-11 (δ_H 1.72 d, J = 15.3 Hz; 1.38 dd, J = 15.3, 9.0 Hz). For the remaining part ($C_9H_9O_7$), HMBC correlations from H_3-7′ (δ_H 1.18 s) to C-2′/C-3′/C-4′, H-1′ (δ_H 4.15 s) to C-3′/C-4′ and H_2-11 to C-1′/C-4′/C-5′ permitted a cyclopentane ring located at C-11 position. Three hydroxy groups were supposed to attach to C-2′, C-4′, and C-5′, respectively, according to the COSY correlation of 5′-OH (δ_H 5.74 s)/H-1′ as well as HMBC signals of 2′-OH to C-1′/C-2′/C-3′ and 4′-OH to C-3′/C-4′/C-5′. Moreover, HMBC correlations from H-1′ to C-6′ and from 4′-OH, to C-6′ suggested a lactone ring formed between C-4′ and C-1′. The final two carbons were assigned to another lactone fused with cyclopentane based on the HMBC correlations of H-8′ (δ_H 3.00 d, J = 18.2 Hz; 2.58 d, J = 18.2 Hz) to C-1′/C-3′/C-9′ and a consideration of molecular formula. Consequently, the planar structure of **1** was deduced (Figure 2).

The *trans*-relationship of rings A and B of the drimane sesquiterpene unit was assigned by the NOESY cross-peaks of H-9/H-5, H_3-13/H-5, and H_3-15/H_3-14,[4c,7,9] which permitted the consistent absolute configurations of C-5/C-9/C-10 as macrophorin A (**3**) based on a biogenetic consideration. For the polyketide part, although there are no useful NOESY correlations among those protons, the cage system limits the number of stereoisomers (**1a**−**1d**) as drawn in Figure 3. An MM2 force field minimization displayed a close distance of H_2-11/H_2-8′ in **1c** and H_2-11/H_3-7′ in **1d**. However, the correlations of H_2-11/H_2-8′ or H_2-11/H_3-7′ were absent in the NOESY spectrum, suggesting stereoisomers **1c** and **1d** were impossible. Subsequently, a theoretical calculation of the NMR data of the isomers **1a** and **1b** revealed that (5*S*,9*S*,10*S*,1′*S*,2′*S*,3′*R*,4′*S*,5′*S*)-**1** (**1a**) had a higher R^2 score and lower deviations (Figure S3), which also gained an almost 100% possibility in a following DP4+ probability analysis (Figure S5).

The complete structure was confirmed by a comparable analysis of calculated and experimental electronic circular dichroism (ECD) spectra, where the same Cotton effects were found in **1a** and the experimental one (Figure 4). Finally, compound **1** was assigned and named alliisativin A.

HRMS analysis of **2** revealed a molecular formula of $C_{24}H_{36}O_6$ suggesting seven degrees of unsaturation. Its NMR data ($CDCl_3$) disclosed resonances attributed to a drimane sesquiterpene unit and a part of $C_9H_{11}O_6$. Diagnostic HMBC correlations observed from H_2-11 (δ_H 2.27 dd, J = 15.4, 9.0 Hz; 1.58 d, J = 9.0 Hz) to C-1′/C-5′/C-6′, H-1′ (δ_H 4.22 br s) to C-3′/C-5′, H-5′ (δ_H 3.17 br s) to C-3′/C-4′ together with the COSY signal of H-1′/H_2-2′ confirmed a cyclohexane ring attached to C-11. In the HMBC spectrum, correlations of H_2-7′ to C-2′/C-3′/C-4′ implied a connection of an oxygenated methylene to C-3′, while correlations of H_2-8′ to C-3′/C-4′/C-5′/C-9′ suggested a C-8′-C-9′ linkage at C-4′. Additionally, two exchangeable protons (δ_H 5.47 br s; δ_H 5.81 s) were found in DMSO-d_6, indicating one hydroxy at C-1′ while the other positioned at C-3′ or C-4′ was evident from the COSY correlations of H-1′/1′-OH and the HMBC cross-peak of the second OH to C-3′, respectively. Considering the chemical shift of C-5′/C-6′ with a comparison of known analogues, an epoxide between C-5′ and C-6′ was deduced.[4c] All this evidence could in principle be attributed to four possible substructures (Figure 5), consisting of a propiolactone (**2a**), an oxetane (**2b**), a butyrolactone (**2c**), or a valerolactone (**2d**). Significantly, analytical scale acetylation of **2** enabled immediate detection of a diacetate, which underwent fast conversion to triacetate within a few hours (Figures S21−S24),

https://doi.org/10.1021/acs.orglett.4c01065
Org. Lett. 2024, 26, 3889−3895

consistent with options **2a** and **2c** (**2b** cannot form triacetate; **2d** would result in monoacetate first). Although the spiropropiolactone in **2a** is chemically unprivileged and extremely unprecedented in literature, a comparable analysis of the chemical shift of C-3′ (evident by HMBC correlations of H-1 to C-3′) in both structures **2a** and **2c** with those of similar compounds was also performed (Figure 6),[10] which strongly suggested that the key carbons in **2c** could match the current chemical shifts (δ_C 84.4 in $CDCl_3$ and δ_C 87.1 in DMSO-d_6). Therefore, the entire planar structure of **2** was established.

The absolute configuration of the drimane moiety was established to be the same as that of **1** and **3** based on NOESY analysis along with the biosynthetic consideration. For the polyketide part, NOESY cross-peaks of H_2-2′b to H-1′ and H_2-7′ indicated H-1′ and H_2-7′ faced toward the same side. However, the relative stereochemistry of C-4′/C-5′/C-6′ could not be determined because of the poor NOESY signals. Subsequently, a theoretical calculation of the NMR data for four isomers followed by a DP4+ probability analysis was performed (Figures S4 and S6), which assigned a 1′*S**,3′*S**,4′*R**,5′*R**,6′*S** configuration for **2**. Fortunately, the empirical inverse octant rule for cyclohexene oxides could be applied to the observed positive Cotton effect at λ_{340nm} ($\Delta\varepsilon$ + 0.02), assigning the absolute configuration of the epoxide as 5′*R* and 6′*S*, which was consistent with a biogenetic relationship with other analogues.[4c,5] Therefore, the structure of compound **2** was determined and named alliisativin B.

Osteoblasts (OBs) and osteoclasts (OCs) are crucial for bone remodeling, and their dysfunction can lead to bone diseases such as osteoporosis and osteosclerosis.[11] Recent research shows that substances produced by these cells can regulate each other's functions, impacting bone resorption and formation.[12] Increasing evidence has suggested that the coupling of OBs and OCs is important for bone therapies.[13] To date, only a few natural products have been found to exhibit therapeutic effects on both OBs and OCs,[14] with just four marine natural products demonstrating this dual activity including hymenialdisine, (3*R**,4*S**)-6,8-dihydroxy-3,4,7-trimethylisocoumarin, sclerotinin C, and asperbiphenyl.[15]

As part of our ongoing search for antiosteoporosis natural products,[15b,16] the two new meroterpenes were tested for their effects on osteoclasts and osteoblasts on bone marrow monocytes (BMMs) and bone mesenchymal stem cells (BMSCs), respectively (Figure 7A). Of note, we found that compound **1** not only suppressed osteoclastogenesis (Figure 7C,D) but also promoted osteogenic mineralization (Figure 7F,G) without cytotoxicity at the concentration up to 10 μM (Figure 7B,E).

Given that compound **1** has dual activity, we constructed a protein−protein interaction (PPI) network of the factors involved in the coupling of osteoblasts and osteoclasts and validated the interaction between the compound and the core target using molecular docking. From the results of PPI, the network consisted of 12 nodes and 16 edges (Figure 8A), in which the top one target of the transforming growth factor beta (TGF-β, TGFB1) was identified as the core target because of its degree value (Figure 8B). TGFB1, an abundant bone matrix protein, is the major coupler of bone resorption to its formation. Its activation helps recruit stem/progenitor cells for tissue regeneration and remodeling processes.[17] Modulating TGF-β signaling has shown promise in treating various conditions like sclerosis, tumor metastasis, osteoarthritis, and osteoporosis.[18] Subsequently, the binding affinity of compound **1** for TGFB1 was assessed using molecular docking techniques. The results of the docking analysis revealed that compound **1** bound to the active pocket of protein 4X2F (Figure 8C,D) through hydrogen bonding with residues LYS213, ARG215, LYS335, and ASN338, as well as hydrophobic interactions with VAL219, LYS337, and LEU340 (Figure 8E,F). The binding activity between PPA and 4X2F was determined to be favorable, with a docking score of −54.302063 kcal/mol (Figure 8E). All this evidence strongly proved that compound **1** effectively targeted the dual active TGFB1 protein, thereby influencing processes related to osteogenesis and osteoclastogenesis.

In conclusion, two novel polyketide-terpenoid hybrid compounds and one known analogue were isolated from the deep-sea-derived fungus *Penicillium allii-sativi* MCCC no. 3A00580. **1** possesses a cage-like tricyclo [2,2,1] ring and exhibited a dual activity in promoting osteogenesis and inhibiting osteoclast, which indicated an antiosteoporosis potential.

■ ASSOCIATED CONTENT

Data Availability Statement

The data underlying this study are available in the published article and its Supporting Information.

Supporting Information

The Supporting Information is available free of charge at https://pubs.acs.org/doi/10.1021/acs.orglett.4c01065.

General experimental procedures (structural assignments were made with additional information from gNOESY, gCOSY, gHSQC, and gHMBC experiments), NMR data and spectra, theoretical calculations, X-ray data, bioassays details, Cartesian coordinates, mass spectra (PDF)

Accession Codes

CCDC 2343652 contains the supplementary crystallographic data for this paper. These data can be obtained free of charge via www.ccdc.cam.ac.uk/data_request/cif, or by emailing data_request@ccdc.cam.ac.uk, or by contacting The Cambridge Crystallographic Data Centre, 12 Union Road, Cambridge CB2 1EZ, UK; fax: +44 1223 336033.

■ AUTHOR INFORMATION

Corresponding Author

Xian-Wen Yang − *Engineering Research Center of Tropical Medicine Innovation and Transformation of Ministry of Education, School of Pharmacy, Hainan Medical University, Hainan Academy of Medical Sciences, Haikou 571199, China; Key Laboratory of Marine Genetic Resources, Third Institute of Oceanography, Ministry of Natural Resources, Xiamen 361005, China;* orcid.org/0000-0002-4967-0844; Email: yangxianwen@tio.org.cn

Authors

Chun-Lan Xie − *Engineering Research Center of Tropical Medicine Innovation and Transformation of Ministry of Education, School of Pharmacy, Hainan Medical University, Hainan Academy of Medical Sciences, Haikou 571199, China; Key Laboratory of Marine Genetic Resources, Third Institute of Oceanography, Ministry of Natural Resources, Xiamen 361005, China; State Key Laboratory of Cellular Stress Biology, Fujian Provincial Key Laboratory of Organ*

https://doi.org/10.1021/acs.orglett.4c01065
Org. Lett. 2024, 26, 3889−3895

and Tissue Regeneration, School of Medicine, Xiamen University, Xiamen 361102, China

Tai-Zong Wu − *Key Laboratory of Marine Genetic Resources, Third Institute of Oceanography, Ministry of Natural Resources, Xiamen 361005, China*

Yuan Wang − *Key Laboratory of Marine Genetic Resources, Third Institute of Oceanography, Ministry of Natural Resources, Xiamen 361005, China*

Robert J. Capon − *Institute for Molecular Bioscience, University of Queensland, Brisbane 4072, Australia;* orcid.org/0000-0002-8341-7754

Ren Xu − *State Key Laboratory of Cellular Stress Biology, Fujian Provincial Key Laboratory of Organ and Tissue Regeneration, School of Medicine, Xiamen University, Xiamen 361102, China*

Complete contact information is available at: https://pubs.acs.org/10.1021/acs.orglett.4c01065

Author Contributions

#Chun-Lan Xie and Tai-Zong Wu contributed equally.

Notes

The authors declare no competing financial interest.

■ ACKNOWLEDGMENTS

This study was financially supported by the National Key Research and Development Program of China (2022YFC2804104) and the Xiamen Southern Oceanographic Center (22GYY007HJ07).

■ REFERENCES

(1) (a) Skropeta, D.; Wei, L. Recent advances in deep-sea natural products. *Nat. Prod. Rep.* **2014**, *31*, 999−1025. (b) Sanchez, J. F.; Somoza, A. D.; Keller, N. P.; Wang, C. C. Advances in *Aspergillus* secondary metabolite research in the post-genomic era. *Nat. Prod. Rep.* **2012**, *29*, 351−371.

(2) (a) Xu, W.; Gavia, D. J.; Tang, Y. Biosynthesis of fungal indole alkaloids. *Nat. Prod. Rep.* **2014**, *31*, 1474−1487. (b) Nakashima, Y.; Mori, T.; Nakamura, H.; Awakawa, T.; Hoshino, S.; Senda, M.; Senda, T.; Abe, I. Structure function and engineering of multifunctional non-heme iron dependent oxygenases in fungal meroterpenoid biosynthesis. *Nat. Commun.* **2018**, *9*, 104. (c) Itoh, T.; Tokunaga, K.; Matsuda, Y.; Fujii, I.; Abe, I.; Ebizuka, Y.; Kushiro, T. Reconstitution of a fungal meroterpenoid biosynthesis reveals the involvement of a novel family of terpene cyclases. *Nat. Chem.* **2010**, *2*, 858−864.

(3) (a) Fang, S. M.; Cui, C. B.; Li, C. W.; Wu, C. J.; Zhang, Z. J.; Li, L.; Huang, X. J.; Ye, W. C. Purpurogemutantin and purpurogemutantidin, new drimenyl cyclohexenone derivatives produced by a mutant obtained by diethyl sulfate mutagenesis of a marine-derived *Penicillium purpurogenum* G59. *Mar. Drugs* **2012**, *10*, 1266−1287. (b) Marco-Contelles, J.; Molina, M. T.; Anjum, S. Naturally occurring cyclohexane epoxides: Sources, biological activities, and synthesis. *Chem. Rev.* **2004**, *104*, 2857−2900.

(4) (a) Marcos, I. S.; Conde, A.; Moro, R. F.; Basabe, P.; Diez, D.; Urones, J. G. Quinone/hydroquinone sesquiterpenes. *Mini-Rev. Org. Chem.* **2010**, *7*, 230−254. (b) Sunassee, S. N.; Davies-Coleman, M. T. Cytotoxic and antioxidant marine prenylated quinones and hydroquinones. *Nat. Prod. Rep.* **2012**, *29*, 513−536. (c) Fu, Y.; Wu, P.; Xue, J. h.; Wei, X. y. Cytotoxic and antibacterial quinone sesquiterpenes from a *Myrothecium* fungus. *J. Nat. Prod.* **2014**, *77*, 1791−1799.

(5) Mohamed, I. E.; Gross, H.; Pontius, A.; Kehraus, S.; Krick, A.; Kelter, G.; Maier, A.; Fiebig, H. H.; Konig, G. M. Epoxyphomalin A and B, prenylated polyketides with potent cytotoxicity from the marine-derived fungus *Phoma* sp. *Org. Lett.* **2009**, *11*, 5014−5017.

(6) Sassa, T.; Ishizaki, A.; Nukina, M.; Ikeda, M.; Sugiyama, T. Isolation and identification of new antifungal macrophorins E, F and G as malonyl meroterpenes from *Botryosphaeria berengeriana*. *Biosci. Biotechnol. Biochem.* **1998**, *62*, 2260−2262.

(7) Tang, M. C.; Cui, X. Q.; He, X. Q.; Ding, Z.; Zhu, T. J.; Tang, Y.; Li, D. H. Late-stage terpene cyclization by an integral membrane cyclase in the biosynthesis of isoprenoid epoxycyclohexenone natural products. *Org. Lett.* **2017**, *19*, 5376−5379.

(8) Sassa, T.; Yoshikoshi, H. New terpene-linked cyclohexenone epoxides, macrophorin A, B and C, produced by the fungus caused *Macrophoma* fruit rot of apple. *Agric. Biol. Chem.* **1983**, *47*, 187−189.

(9) (a) Fujimoto, H.; Nakamura, E.; Kim, Y. P.; Okuyama, E.; Ishibashi, M.; Sassa, T. Immunomodulatory constituents from an Ascomycete, *Eupenicillium crustaceum*, and revised absolute structure of macrophorin D. *J. Nat. Prod.* **2001**, *64*, 1234−1237. (b) Garai, S.; Mehta, G. Total synthesis of bioactive drimane-epoxyquinol hybrid natural products: macrophorin A, 4'-oxomacrophorin, A, and 1'-epi-craterellin A. *Tetrahedron Lett.* **2014**, *55*, 6252−6256.

(10) (a) Yu, H.; Sperlich, J.; Höfert, S.-P.; Janiak, C.; Teusch, N.; Stuhldreier, F.; Wesselborg, S.; Wang, C.; Kassack, M. U.; Dai, H.; Liu, Z.; Proksch, P. Azaphilone pigments and macrodiolides from the coprophilous fungus Coniella fragariae. *Fitoterapia* **2019**, *137*, 104249. (b) Zhu, X.; Xia, D.; Zhou, Z.; Xie, S.; Shi, Z.; Chen, G.; Wang, L.; Pan, K. Lycosquarrines A−R, lycopodium alkaloids from *Phlegmariurus squarrosus*. *J. Nat. Prod.* **2020**, *83*, 2831−2843. (c) Wang, X. N.; Bashyal, B. P.; Wijeratne, E. M. K.; U'Ren, J. M.; Liu, M. X.; Gunatilaka, M. K.; Arnold, A. E.; Gunatilaka, A. A. L. Smardaesidins A−G, isopimarane and 20-*nor*-isopimarane diterpenoids from *Smardaea* sp., a fungal endophyte of the moss *Ceratodon purpureus*. *J. Nat. Prod.* **2011**, *74*, 2052−2061. (d) Niu, S.; Liu, Q.; Xia, J. M.; Xie, C. L.; Luo, Z. H.; Shao, Z.; Liu, G. M.; Yang, X. W. Polyketides from the deep-sea-derived fungus *Graphostroma* sp. MCCC 3A00421 showed potent antifood allergic activities. *J. Agric. Food Chem.* **2018**, *66*, 1369−1376.

(11) (a) Reid, I. R.; Billington, E. O. Drug therapy for osteoporosis in older adults. *Lancet.* **2022**, *399*, 1080−1092. (b) Wang, L. J.; You, X. L.; Zhang, L. L.; Zhang, C. Q.; Zou, W. G. Mechanical regulation of bone remodeling. *Bone Res.* **2022**, *10*, 16.

(12) (a) Furuya, M.; Kikuta, J.; Fujimori, S.; Seno, S.; Maeda, H.; Shirazaki, M.; Uenaka, M.; Mizuno, H.; Iwamoto, Y.; Morimoto, A. Direct cell-cell contact between mature osteoblasts and osteoclasts dynamically controls their functions *in vivo*. *Nat. Commun.* **2018**, *9*, 300. (b) Salhotra, A.; Shah, H. N.; Levi, B.; Longaker, M. T. Mechanisms of bone development and repair. *Nat. Rev. Mol. Cell Biol.* **2020**, *21*, 696−711.

(13) (a) Li, X.; Wang, L.; Huang, B.; Gu, Y.; Luo, Y.; Zhi, X.; Hu, Y.; Zhang, H.; Gu, Z.; Cui, J.; Cao, L.; Guo, J.; Wang, Y.; Zhou, Q.; Jiang, H.; Fang, C.; Weng, W.; Chen, X.; Chen, X.; Su, J. Targeting actin-bundling protein L-plastin as an anabolic therapy for bone loss. *Sci. Adv.* **2020**, *6*, No. eabb7135. (b) Liu, R. X.; Gu, R. H.; Li, Z. P.; Hao, Z. Q.; Hu, Q. X.; Li, Z. Y.; Wang, X. G.; Tang, W.; Wang, X. H.; Zeng, Y. K.; Li, Z. W.; Dong, Q.; Zhu, X. F.; Chen, D.; Zhao, K. W.; Zhang, R. H.; Zha, Z. G.; Zhang, H. T. Trim21 depletion alleviates bone loss in osteoporosis via activation of YAP1/β-catenin signaling. *Bone Res.* **2023**, *11*, 56.

(14) (a) El-Desoky, A. H. H.; Tsukamoto, S. Marine natural products that inhibit osteoclastogenesis and promote osteoblast differentiation. *J. Nat. Med.* **2022**, *76*, 575−583. (b) Wang, Q. Q.; Chen, D. L.; Jin, H. M.; Ye, Z.; Wang, C.; Chen, K.; Kuek, V.; Xu, K.; Qiu, H.; Chen, P.; Song, D. Z.; Zhao, J. M.; Liu, Q.; Davis, R. A.; Song, F. M.; Xu, J. K. Hymenialdisine: a marine natural product that acts on both osteoblasts and osteoclasts and prevents estrogen-dependent bone loss in mice. *J. Bone Miner. Res.* **2020**, *35*, 1582−1596.

(15) (a) Chaugule, S. R.; Indap, M. M.; Chiplunkar, S. V. Marine natural products: New avenue in treatment of osteoporosis. *Front. Mar. Sci.* **2017**, *4*, 384. (b) Zhang, Y.; Xie, C. L.; Wang, Y.; He, X. W.; Xie, M. M.; Li, Y.; Zhang, K.; Zou, Z. B.; Yang, L. H.; Xu, R.; Yang, X. W. Penidihydrocitrinins A-C: New polyketides from the deep-sea-derived *Penicillium citrinum* W17 and their anti-Inflammatory and anti-osteoporotic bioactivities. *Mar. Drugs* **2023**, *21*, 538.

(16) (a) He, Z. H.; Xie, C. L.; Wu, T.; Yue, Y. T.; Wang, C. F.; Xu, L.; Xie, M. M.; Zhang, Y.; Hao, Y. J.; Xu, R.; Yang, X. W. Tetracyclic steroids bearing a bicyclo[4.4.1] ring system as potent antiosteoporosis agents from the deep-sea-derived fungus *Rhizopus* sp. W23. *J. Nat. Prod.* **2023**, *86*, 157−165. (b) He, Z. H.; Xie, C. L.; Wu, T.; Zhang, Y.; Zou, Z. B.; Xie, M. M.; Xu, L.; Capon, R. J.; Xu, R.; Yang, X. W. Neotricitrinols A-C, unprecedented citrinin trimers with anti-osteoporosis activity from the deep-sea-derived *Penicillium citrinum* W23. *Bioorg. Chem.* **2023**, *139*, 106756. (c) Xie, C. L.; Yue, Y. T.; Xu, J. P.; Li, N.; Lin, T.; Ji, G. R.; Yang, X. W.; Xu, R. Penicopeptide A (PPA) from the deep-sea-derived fungus promotes osteoblast-mediated bone formation and alleviates ovariectomy-induced bone loss by activating the AKT/GSK-3β/β-catenin signaling pathway. *Pharmacol. Res.* **2023**, *197*, 106968.

(17) (a) Sims, N. A.; Martin, T. J. Osteoclasts provide coupling signals to osteoblast lineage cells through multiple mechanisms. *Annu. Rev. Physiol.* **2020**, *82*, 507−529. (b) Edwards, J. R.; Nyman, J. S.; Lwin, S. T.; Moore, M. M.; Esparza, J.; O'Quinn, E. C.; Hart, A. J.; Biswas, S.; Patil, C. A.; Lonning, S.; Mahadevan-Jansen, A.; Mundy, G. R. Inhibition of TGF-β signaling by 1D11 antibody treatment increases bone mass and quality *in vivo*. *J. Bone Miner. Res.* **2010**, *25*, 2419−2426.

(18) (a) Xu, X.; Zheng, L. W.; Yuan, Q.; Zhen, G. H.; Crane, J. L.; Zhou, X. D.; Cao, X. Transforming growth factor-β in stem cells and tissue homeostasis. *Bone Res.* **2018**, *6*, 2. (b) Weivoda, M. M.; Ruan, M.; Pederson, L.; Hachfeld, C.; Davey, R. A.; Zajac, J. D.; Westendorf, J. J.; Khosla, S.; Oursler, M. J. Osteoclast TGF-β receptor signaling Induces Wnt1 secretion and couples bone resorption to bone formation. *J. Bone Miner. Res.* **2016**, *31*, 76−85.

https://doi.org/10.1021/acs.orglett.4c01065
Org. Lett. 2024, 26, 3889−3895